Reliability-centered Planning with Geographic Graph Constraints for Feeder Routing and Conductor Sizing

Zhengbo Li, Youbo Liu, *Member*, *IEEE*, Yue Xiang, Haolan Yang, Lingfeng Wang, and Junyong Liu, *Member*, *IEEE*

***Abstract*—Feeder routing and reliability assessment are essential for effective distribution network planning. However, excessively long feeders can lead to increased costs and decreased reliability. To enhance economic and reliability performance, this paper proposes a reliability-centered planning method for feeder routing and conductor sizing. Specifically, a graph-based fictitious power flow model is constructed within the geographic graph. Overlapping feeder routes powered by fictitious power flows from multiple sources are designated as line connection. These feeder routes, constrained by the geographic graph, are interconnected via line connection to form a mesh network structure. To meet the requirements of reliability-centered optimization, the affiliation variables are introduced. Based on the affiliation variables, the algebraic formula is embedded into the fictitious power flow model to enable the calculation of reliability during the optimization process. By incorporating customized reliability-related constraints in the model, the specific reliability objectives can be achieved. In addition, the non-convex terms in the fictitious power flow model are relaxed into convex forms, and certain variable products are replaced with auxiliary variables, allowing the problem to be solved by an off-the-shelf solver. Finally, the proposed method is tested on two case studies, demonstrating its effectiveness.**

***Index Terms*—Distribution network planning, analytical reliability assessment, feeder routing, geographic graph, mixed-integer linear programming (MILP), conductor sizing.**

NOMENCLATURE

A. Indices and Sets

Ω	Set of load levels
a	Index of conductors
A	Set of conductors
b	Index of load levels
B	Set of all possible edges of representing graph
B_i^{end}	Set of edges ending at node i
B^{source}	Set of all edges directly connected to a substation (source) node
B_i^{start}	Set of edges starting at node i
i, j, z	Indices of nodes
ij, ji, xy	Indices of branches
N	Set of all nodes of representing graph
N^{load}	Set of load nodes
N^{source}	Set of substation (source) nodes

B. Parameters

α_{ij}^{+}	Indication of power flow in direction of edge ij
α_{ij}^{-}	Indication of power flow in direction of edge ji
δ	Interest rate
Δ_b	Duration of load level b
$\varepsilon_i^{\text{CID}}$	Customer interruption duration (CID) requirement of node i
$\varepsilon_i^{\text{CIF}}$	Customer interruption frequency (CIF) requirement of node i
λ_{ij}	Unitary failure rate of edge ij
μ	Cost coefficient for expected energy not supplied under branch outages
μ_b	Loading factor of load level b
τ_{ij}^{RS}	Duration of repair-and-switching interruptions associated with failure of edge ij
τ_{ij}^{SO}	Duration of switching-only interruptions associated with failure of edge ij
ω	Present worth factor calculated by δ over a period of t years
$c_a^{\text{conductor}}$	Investment cost of conductor type a
$c_a^{\text{maintenance}}$	Maintenance cost of conductor type a
d_{ij}	Length of edge ij
$I_a^{\max}$	Thermal limit of conductor type a
M	A sufficiently large positive constant
NC_i	Number of customers at node i

Manuscript received: August 8, 2024; revised: December 20, 2024; accepted: March 12, 2025. Date of CrossCheck: March 12, 2025. Date of online publication: March 27, 2025.

This work was supported by the National Nature Science Foundation of China (No. 51977133).

Z. Li, Y. Liu (corresponding author), Y. Xiang, H. Yang, and J. Liu are with the College of Electrical Engineering, Sichuan University, Chengdu 610065, China (e-mail: lizhengbo@stu.scu.edu.cn; liuyoubo@scu.edu.cn; xiang@scu.edu.cn; 2024323035010@stu.scu.edu.cn; liujy@scu.edu.cn).

L. Wang is with the Department of Electrical Engineering and Computer Science, University of Wisconsin-Milwaukee, Milwaukee, WI 53211, USA (e-mail: l.f.wang@ieee.org).

DOI: 10.35833/MPCE.2024.000884

P_i^{load} Active load demand of node i

Q_i^{load} Reactive load demand of node i

r_{ij}^a Resistance of edge ij for conductor type a

$S_a^{\max}$ Capacity of conductor type a

t Planning stage

$V^{\max}$ The maximum voltage limit for nodes

$V^{\min}$ The minimum voltage limit for nodes

x_{ij}^a Reactance of edge ij for conductor type a

C. Binary Variables

f_{ij}^- Binary variable equal to 1 when transmitting fictitious power flow along ji direction

f_{ij}^+ Binary variable equal to 1 when transmitting fictitious power flow along ij direction

f_{ij} Binary variable equal to 1 when transmitting fictitious power flow on edge ij

k_{xy}^{ij} Binary variable equal to 1 when edge xy is in a feeder whose first edge is ij, and 0 otherwise

n_i Binary variable equal to 1 when transmitting fictitious power through node i

Y_{ij}^a Binary variable equal to 1 when conductor type a is installed at edge ij

D. Continuous Variables

Γ_i^{RS} Expected duration of repair-and-switching interruptions affecting node i

Γ_i^{SO} Expected duration of switching-only interruptions affecting node i

Π_i^{RS} Expected rate of repair-and-switching interruptions affecting load node i

Π_i^{SO} Expected rate of switching-only interruptions affecting load node i

$ASAI$ Average system availability index

c_{I} Installation cost

CID_i CID at node i

CIF_i CIF at node i

c_{M} Maintenance cost

c_{R} Reliability cost

$EENS$ Expected energy not supplied

I_{ij}^+, I_{ij}^- Square currents along edges ij and ji

$I_{ij}^{\max}$ Thermal limit of edge ij when conductor type a is installed

m_{ij}^a Average annual maintenance cost of conductor type a on edge of ij

P_{ij}^-, Q_{ij}^- Fictitious active and reactive power flowing along edge ji

P_{ij}^+, Q_{ij}^+ Fictitious active and reactive power flowing along edge ij

P_i^{g}, Q_i^{g} Injected active and reactive power at generation source node i

P_i^{out}, Q_i^{out} Fictitious active and reactive power flowing out from node i

Pr_{ij}^+, Qx_{ij}^+, Ir_{ij}^+, Ix_{ij}^+, Pr_{ij}^-, Qx_{ij}^-, Ir_{ij}^-, Ix_{ij}^-, Irx_{ij}^+, Irx_{ij}^- Auxiliary variables used to replace product of two variables such as $P_{ij}^+ \times r_{ij}$, $Q_{ij}^+ \times x_{ij}$, $I_{ij}^+ \times r_{ij}$, $I_{ij}^+ \times x_{ij}$, $I_{ij}^+ \times (r_{ij}^2 + x_{ij}^2)$

r_{ij}, x_{ij} Resistance and reactance of edge ij

s_{ij}^a Unit length installation cost of conductor type a on edge ij

$SAIDI$ System average interruption duration index

$SAIFI$ System average interruption frequency index

$S_{ij}^{\max}$ Capacity of edge ij when conductor a is installed

V_i Square voltage at node i

$V_i^{\max}$, $V_i^{\min}$ Upper and lower limits of nodal voltage for feeder connected nodes

I. Introduction

FEEDER routing (FR) optimization plays an important role in achieving the economical and reliable performance of power distribution networks [1]. The FR optimization is complicated due to the large number of variables and constraints related to geographic characteristics, reliability evaluation, electrical criteria, etc. According to these problems, existing research works [1], [2] usually plan the spatial network layout based on geographic information systems (GISs), followed by security and reliability verifications. However, the reliability evaluation is carried out after determining the spatial network layout, attempting to reduce the computational complexity in problem solving. The absence of reliability consideration in FR optimization may lead to the uncontrolled reliability performance of the planning results. For instance, [3]-[5] overlook the reliability evaluation during the optimization process, resulting in a solution with low reliability. To address the issue of low reliability expectations, [6] calculates the reliability indices and associated costs for each solution based on the regulatory model, providing decision-makers with a diverse set of plans for selection. However, [6] fails to influence the network layout designed in the sequential process, consequently yielding a locally optimal solution. On the other hand, simulation-based methods are implemented by alternating optimization and reliability evaluation to generate feasible solutions, which involve a massive number of iterations [7]. Consequently, this method entails a significant computational burden due to the excessive number of iterations required. Besides the computational burden, these posterior reliability evaluation methods also fail to meet customized reliability requirements in the optimization process.

To overcome the defects of massive computing tasks and inaccurate reliability evaluation, some linear formula-based algebraic reliability assessment methods have been proposed in [8]-[10], which can be combined with electrical conditions in the planning model. In [11], a reliability evaluation method based on linear programming is proposed, where the

fictitious power flow is modeled to derive system reliability indices under specific fault interruptions. Inspired by [11], a mixed-integer linear programming (MILP) model of FR incorporating reliability criteria is proposed in [12], where the reliability evaluation method is applied during the optimizing process. In the MILP model, the common reliability indices such as the system average interruption frequency index (SAIFI), the system average interruption duration index (SAIDI), the average service availability index (ASAI), and the expected energy not supplied (EENS) are constrained in the optimization process, and EENS is added to the objective function multiplied by a weighting coefficient. However, the post-fault load restoration strategies between feeders are not considered in this method, which may lead to overinvestment for specific reliability requirements. To further formulate the calculation of reliability indices considering post-fault load restoration, [10] presents an algebraic method for the analytical predictive reliability evaluation, which calculates the standard network-dependent reliability indices without simulation or optimization. Based on [10], a multi-stage distribution network expansion planning model is proposed in [8], which models the economic reward-penalty scheme for lessening the gap between the theoretical and real reliability costs. Nevertheless, these methods [8], [12] neglect the spatial network layout requirements, which may affect the economic and reliability performances in graph-based planning [13], [14]. References [15] and [16] apply the raster map to integrate optimal electrical line routing and network reliability evaluation by defining line linkages as power flow direction variables in the network-dependent reliability evaluation. However, the reliability-related constraints and reliability-centric objective function are not taken into consideration. It is unable to enhance the reliability in spatial network planning. Similarly, embedded reliability constraints are still rarely applied in the existing graph-based planning models due to the complexity of integrating algebraic reliability formulas. This complexity is caused by the lack of essential relationships between different branches.

To reduce the complexity, several methods integrating algebraic reliability formulas with geographical constraints have been proposed [17]. Additionally, this paper introduces a reliability-centered planning method for optimal FR and conductor sizing. This paper models fictitious power flow and implements reliability evaluation on the edges of the graph, which improves the spatial layout and reliability in the optimization process. Then, the mesh layout requirement would be satisfied by connecting the feeder routes powered from diverse sources. Meanwhile, the conductor sizes are determined through the maximum fictitious power flow on each edge. In contrast to the graph-based FR followed by security verification and reliability re-evaluation, the proposed method adds the reliability-centered objective function and constraints through the affiliation variable to the fictitious power flow model. Furthermore, the reliability calculation is performed by integrating affiliation variables and algebraic formulas, which significantly enhances the spatial network layout. Finally, various methods in this paper and [2]-[9], [11], [14]-[18] are compared, as shown in Table I, showing that this paper can provide a comprehensive planning method for FR and conductor sizing considering reliability requirement and geographic constraints.

TABLE I
COMPARISON OF DIFFERENT METHODS FOR GRAPH-BASED FR AND CONDUCTOR SIZING WITH RELIABILITY CONSTRAINTS

Method	Technique	Reliability assessment	Graph-based FR	Conductor sizing
[2], [7]	Metaheuristics	Simulation		Optimized in objective function
[4]	Metaheuristics		Automatic street map generation	
[6]	Heuristics	Simulation		
[3], [5]	Mathematical programming		Subgraph of discretized map	Optimized in objective function
[8], [9]	Mathematical programming	Analytical method		
[11], [15]	Mathematical programming	Linear programming		Obtained via model constraints
[14], [16]	Mathematical programming	Linear programming	Gathering based on alternative routes	
[17], [18]	Mathematical programming	Analytical method	Optimized in model	
This paper	Mathematical programming	Linear programming	Subgraph of discretized map	Obtained via model constraints

The major contributions of this paper are listed as follows.

1) A graph-based fictitious power flow model is developed, which replaces the lines of the power grid with the edges in geographic graph. These discrete edges are utilized to splice into feeder routes, while certain geographic graph-constrained edges are removed to meet realistic requirements.

2) The overlapping feeder routes with fictitious power flows from multiple sources are designed as line connection, connecting the radial network into the mesh network. Moreover, the conductor sizing is optimized through the thermal stability limit on each edge, improving the economic efficiency of planning.

3) The affiliation variable is introduced to define the upstream and downstream relationships between edges, facilitating the integration of algebraic reliability formulas within the model. Customized reliability requirements are achieved by incorporating specific reliability index constraints into the model through calculation formulas.

The remainder of this paper is organized as follows. Section II introduces the problem statement in which the associated assumptions for graph-based fictitious power flow model and reliability calculation are described. Section III details the fictitious power flow model based on mixed-integer second-order cone programming (MISOCP) in the geographic

graph. Section IV emphasizes the process of improving the model by using affiliation variables and algebraic reliability formulas. Section V conducts case study on two test systems. Finally, Section VI concludes this paper.

II. Problem Statement

As demonstrated in [5], FR optimization without geographic constraints may result in doubled feeder length. To avoid excessive costs caused by lengthy feeders, this paper embeds geographic constraints into the fictitious power flow model through a geographic graph. Specifically, the proposed method treats each edge of the geographic graph as an independent candidate, with its selection determined by solving the FR optimization. The feeders would be routed along graph edges that meet realistic requirements, including spatial conditions and mesh layout constraints. However, a significant challenge lies in integrating reliability evaluation into the fictitious power flow model. To address this, we add the existing algebraic reliability formulas into the fictitious power flow model, realizing a reliability-centered planning optimization [10]. The reliability formulas rely on network topology and power flow direction during the optimization process. But there is no predefined upstream/downstream relationship among the edges during problem solving. Consequently, the proposed method introduces affiliation variables to represent the upstream/downstream relationship, enabling the integration of reliability formulas into the fictitious power flow model. Moreover, the reliability calculation with customized reliability constraints are implemented through these affiliation variables, which will be detailed in Section IV.

A. Assumptions

To implement FR optimization with geographic graph constraints, a representative geographic graph is constructed in the Euclidean plane to simulate the actual geographic graph, as illustrated in Fig. 1(a). On the two-dimensional Euclidean plane, the vertices and edges correspond to the nodes and wiring of the circuit, respectively. In the geographic graph, the vertices are categorized into three types: normal nodes, substation nodes, and load nodes, based on the presence of substations or loads in their vicinity. Moreover, edges transferring power in the fictitious power flow must be equipped with an appropriate conductor size to ensure the load demand and cost effectiveness. Specifically, the vertices and edges in FR are also required to meet the following conditions and assumptions, based on the geographic graph constraints and security limits.

1) To illustrate the characteristics of spatial FR, a simple grid plane graph is shown in Fig. 1(a). For vertices without substation or load around them, they are deemed as normal nodes. Except for the vertices, the feeders and branches of the distribution network are replaced by discrete edges in the grid plane graph. To distinguish the opposite power flow directions on the same branch of different topologies, two reference directions are set for each edge. Only one direction functions when the distribution network radially operates. On the other hand, two directions may respectively function in diverse topologies. For the network reconfiguration, feeders are assumed to be equipped with circuit breakers and both ends of each branch are also assumed to be equipped with switches, as shown in Fig. 1(a). Once the fault occurs, the distribution network performs topology reconfiguration through tie-lines to ensure the supply of the load, where the power transferred from different sources may flow in different directions on the same branch.

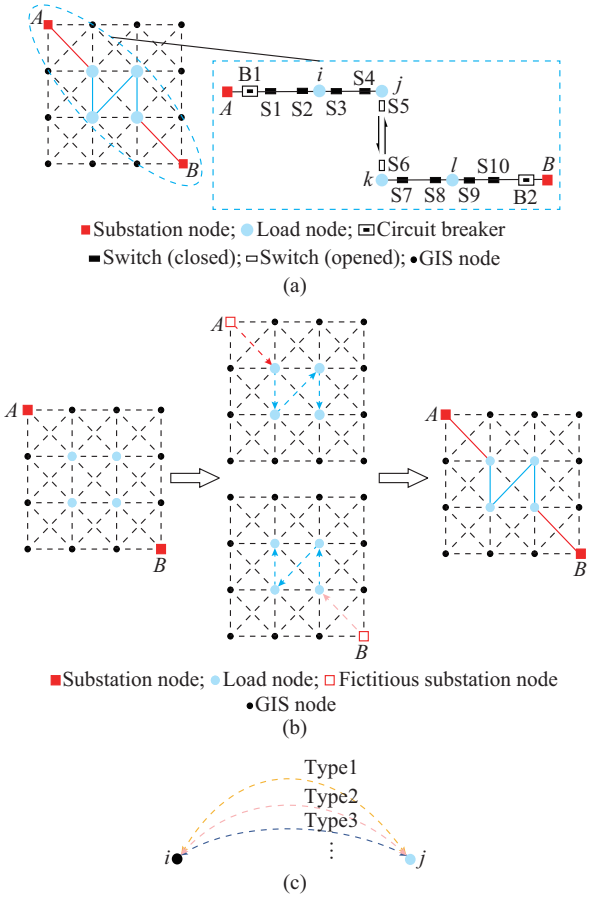

Fig. 1. Feeder planning and type selection process. (a) Geographic graph constructed in Euclidean plane. (b) Two fictitious power flows of mesh network. (c) Various conductor sizes for one edge.

2) To ensure the operational security of selected edges supplied by an individual substation, the fictitious power flow is modeled on the edges to simulate the power transmission between two adjacent vertices. Through power transmission edges carrying fictitious power flow, the normal nodes, load nodes, and substation nodes are interconnected in a radial configuration. To meet the mesh requirement, the proposed method models fictitious power flow for all substations. All the edges carrying power flow originating from various substations form a mesh network topology, ensuring reliable power transmission. Therefore, this paper introduces the fictitious power flow model according to the number of substations. For instance, a mesh network is shown in Fig. 1(b) with two substations and two fictitious power flows. Meanwhile, the red and blue dotted edges represent the fictitious power flows. The substation node supplies power through these edges. Finally, all the edges applied in the fictitious power flow are selected in the distribution network

planning.

3) The edges applied in FR should be equipped with a suitable conductor size. As shown in Fig. 1(c), it is assumed that there are various conductor sizes to be selected for an edge. Each conductor type has its unique thermal stability limit. To ensure the safe operation, only one conductor size will be determined for the edge by optimizing multiple fictitious power flows among the substations. Specifically, once an edge is applied to FR, the conductor size on the edge should be selected as the type with an adequately large capacity to meet the requirements of safe operation.

B. Reliability Assessment Descriptions

It is assumed that the feeders and branches of the distribution network are equipped with circuit breakers and switches. When a fault occurs, the first circuit breaker upstream the fault trips to isolate the fault. After the switching-only interruption, switches and circuit breakers are operated to reconfigure the network topology to curtail the unsupplied energy. In [10], for repair-and-switching interruptions, the distribution network should restore the power supply after the fault recovery. Different from the repair-and-switching interruptions, the switching-only interruptions only need time to isolate the faulted components and reconfigure the topology. Based on the above two situations, the existing algebraic method can be used to formulate the calculation of reliability indices. Then, according to the method proposed in [11], the reliability indices such as customer interruption duration (CID), customer interruption frequency (CIF), SAIFI, SAIDI, ASAI, and EENS of the distribution network under the fixed topology are also calculated using the algebraic formulas, which are not repeated in this paper due to space limit. But the analytical reliability expressions under different conditions are shown in Fig. 2, and the reliability calculation is represented as:

$$\begin{cases} \sum_{ji\in B}\alpha_{ji}^{+}+\sum_{ji\in B}\alpha_{ji}^{-}=0 \quad \forall i\in N^{\text{source}} \\ \sum_{ji\in B}\alpha_{ji}^{+}+\sum_{ji\in B}\alpha_{ji}^{-}=1 \quad \forall i\in N^{\text{source}} \\ \alpha_{ij}^{+}+\alpha_{ij}^{-}=1 \quad \forall (i,j)\in B \end{cases} \tag{1}$$

$$\Pi_i^{\text{RS}}=\Pi_j^{\text{RS}}+\lambda_{ij}d_{ij}\alpha_{ij}^{-}-\lambda_{ij}d_{ij}\alpha_{ij}^{+} \quad \forall (i,j)\in B \tag{2}$$

$$\Pi_i^{\text{SO}}=\Pi_j^{\text{SO}}+\lambda_{ij}d_{ij}\alpha_{ij}^{+}-\lambda_{ij}d_{ij}\alpha_{ij}^{-} \quad \forall (i,j)\in B, i,j\notin N^{\text{source}} \tag{3}$$

$$\Gamma_i^{\text{RS}}=\Gamma_j^{\text{RS}}+\tau_{ij}^{\text{RS}}\lambda_{ij}d_{ij}\alpha_{ij}^{-}-\tau_{ij}^{\text{RS}}\lambda_{ij}d_{ij}\alpha_{ij}^{+} \quad \forall (i,j)\in B, i,j\notin N^{\text{source}} \tag{4}$$

$$\Gamma_i^{\text{SO}}=\Gamma_j^{\text{SO}}+\tau_{ij}^{\text{SO}}\lambda_{ij}d_{ij}\alpha_{ij}^{+}-\tau_{ij}^{\text{SO}}\lambda_{ij}d_{ij}\alpha_{ij}^{-} \quad \forall (i,j)\in B, i,j\notin N^{\text{source}} \tag{5}$$

$$CIF_i=\Pi_i^{\text{RS}}+\Pi_i^{\text{SO}} \quad \forall i\in N^{\text{load}} \tag{6}$$

$$CID_i=\Gamma_i^{\text{RS}}+\Gamma_i^{\text{SO}} \quad \forall i\in N^{\text{load}} \tag{7}$$

$$SAIFI=\sum_{i\in N^{\text{load}}}NC_i\cdot CIF_i\Big/\sum_{i\in N^{\text{load}}}NC_i \tag{8}$$

$$SAIDI=\sum_{i\in N^{\text{load}}}NC_i\cdot CID_i\Big/\sum_{i\in N^{\text{load}}}NC_i \tag{9}$$

$$ASAI=1-SAIDI/8760 \tag{10}$$

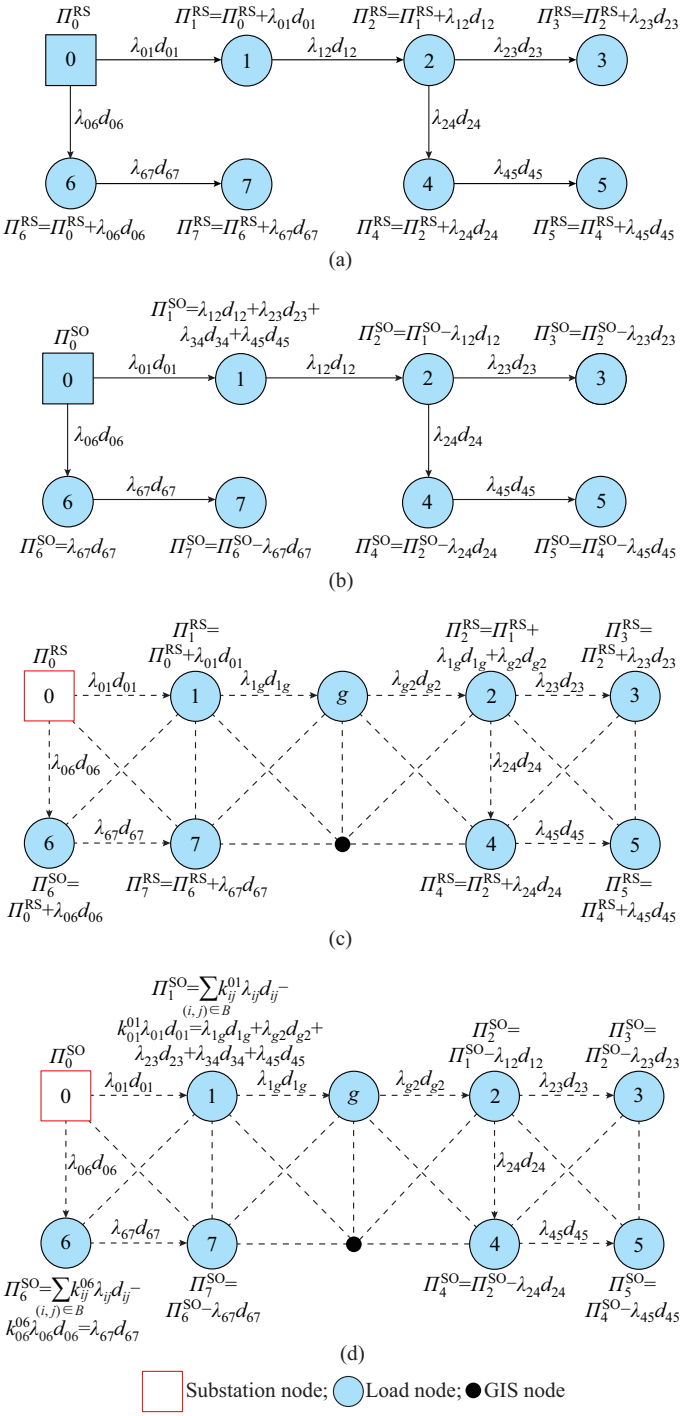

Fig. 2. Illustrative examples of analytical reliability expressions. (a) Analytical reliability calculation of repair-and-switching interruptions without geographic graph. (b) Analytical reliability calculation of switching-only interruptions without geographic graph. (c) Analytical reliability calculation of repair-and-switching interruptions with geographic graph. (d) Analytical reliability calculation of switching-only interruptions with geographic graph.

$$EENS=\sum_{b\in\Omega}\frac{\Delta_b}{8760}\sum_{i\in N^{\text{load}}}CID_i\cdot\mu_b D_i \tag{11}$$

In Fig. 2(a) and (b), the existing calculation methods apply the power flow direction (α_{ij}^{+} and α_{ij}^{-}) of each branch in the fixed topology to calculate the reliability indices for repair-and-switching interruptions and switching-only interrup-

tions, respectively. In Fig. 2(a), the expected rate of repair-and-switching interruptions affecting load node i (Π_i^{RS}) should be calculated by (2), e.g., $\Pi_2^{\mathrm{RS}}=\Pi_1^{\mathrm{RS}}+\lambda_{12}d_{12}$. However, the feeders and branches are replaced by edges in the geographic graph. In Fig. 2(c), branch $(1,2)$ between two load nodes is divided into two edges $(1,g)$ and $(g,2)$. Thus, the reliability calculation changes accordingly, and $\Pi_2^{\mathrm{RS}}=\Pi_1^{\mathrm{RS}}+\lambda_{12}d_{12}\alpha_{12}^{+}$ is replaced by $\Pi_2^{\mathrm{RS}}=\Pi_1^{\mathrm{RS}}+\lambda_{1g}d_{1g}\alpha_{1g}^{+}+\lambda_{g2}d_{g2}\alpha_{g2}^{+}$, where $\alpha_{12}^{+}=1$ is changed to $\alpha_{1g}^{+}=1$, $\alpha_{g2}^{+}=1$. Moreover, to integrate the formula into the fictitious power flow model, the power flow directions α_{ij}^{+} and α_{ij}^{-} of branches should also be replaced by the fictitious power flow directions f_{ij}^{+} and f_{ij}^{-} of the edges, respectively, and $\lambda_{1g}d_{1g}\alpha_{1g}^{+}$ and $\lambda_{g2}d_{g2}\alpha_{g2}^{+}$ are changed to $f_{1g}^{+}\lambda_{1g}d_{1g}$ and $f_{g2}^{+}\lambda_{g2}d_{g2}$, respectively. However, it is not sufficient to only replace the fictitious power flow direction to integrate the reliability calculation of the switching-only interruption into the fictitious power flow model. For example, it is unable to calculate the reliability indices of switching-only interruptions affecting nodes near the substation like Π_1^{SO} and Π_6^{SO} in the solving process, as they are merely related to their downstream edges that are undetermined in the optimization. Thus, this paper introduces the affiliation variable k_{ij}^{ij} to represent the upstream and downstream relationship between edges. In Fig. 2(d), the edge (6, 7) is the downstream of the edge $(0,6)$ and is represented by $k_{67}^{06}=1$. In addition, for the affiliation of edge $(0,6)$ and other edges except $(6,7)$, the affiliation variables $k_{ij}^{06}=0$, $(i,j)\in B$, $(i,j)\neq(0,6)$. If the edge (i,j) is selected during the optimization process, k_{ij}^{ij} will be 1, such as $k_{06}^{06}=1$. Therefore, based on the affiliation variables, the formulas of switching-only interruptions affecting nodes near the substation in Fig. 2(b) are reformulated as constraints and embedded into the graph-based fictitious power flow model. As an illustration, $\Pi_1^{\mathrm{SO}}=\lambda_{12}d_{12}+\lambda_{23}d_{23}+\lambda_{34}d_{34}+\lambda_{45}d_{45}$ and $\Pi_6^{\mathrm{SO}}=\lambda_{67}d_{67}$ are changed to $\Pi_1^{\mathrm{SO}}=\sum_{(i,j)\in B}k_{ij}^{01}\lambda_{ij}d_{ij}-k_{01}^{01}\lambda_{01}d_{01}$ and $\Pi_6^{\mathrm{SO}}=\sum_{(i,j)\in B}k_{ij}^{06}\lambda_{ij}d_{ij}-k_{06}^{06}\lambda_{06}d_{06}$, respectively. Then, the reliability-related parameters representing the rate and duration of interruptions are applied to (6)-(11) to calculate the reliability indices. By embedding these equations, the customized reliability requirements can be set as constraints in the fictitious power flow model. The modeling process and the reliability constraints based on these formulas are discussed in Section IV.

III. Fictitious Power Flow Model

As demonstrated in Section II-A, when modeling on a geographic graph, the branches of the distribution network are replaced by discrete edges. Consequently, the branch power is substituted with edge power. This paper has modified the branch-based power flow constraints in the second-order cone programming (SOCP), and represents the edge-based power flow constraints proposed in Section III-C. This power flow constraint ensures that the power flow model for FR is constructed based on the fictitious model, which is a convex SOCP. Moreover, by introducing integer variables in the conductor size constraints in Section III-B, the proposed model is transformed into an MISOCP.

A. Objective Function

The objective function for the proposed model consists of three components: the installation cost c_{I}, the maintenance cost c_{M}, and the reliability cost c_{R}. c_{I} and c_{M} mainly depend on the feeder length and the conductor size, where the cost per unit length differs for differing conductor sizes [18]. Moreover, the reliability cost c_{R} is defined as the product of the reliability index *EENS* and the unit reliability cost of EENS μ. The objective function C with three investment components is presented by:

$$\min C=c_{\mathrm{I}}+c_{\mathrm{M}}+c_{\mathrm{R}}=\sum_{(i,j)\in B}\left(d_{ij}\sum_{a\in A}s_{ij}^{a}\right)+\omega\left[\sum_{(i,j)\in B}\left(d_{ij}\sum_{a\in A}m_{ij}^{a}\right)+\mu\cdot EENS\right] \tag{12}$$

$$\omega=\frac{(1+\delta)^{t}-1}{\delta(1+\delta)^{t}} \tag{13}$$

B. Conductor Size Constraints

Based on the assumption in Section II-A, the fictitious power flow direction variables are specified for each edge in the model as two binary variables f_{ij}^{+}, f_{ij}^{-}. The binary variable f_{ij}^{+} indicates that the flow direction is the same as the reference direction (from i to j), and the binary variable f_{ij}^{-} indicates that the fictitious flow from j to i is opposite to f_{ij}^{+}. Once the power is transferred by the edge (i,j) in the fictitious power flow, the edge (i,j) would be selected. The selectable conductor size for each edge must be chosen from a predefined set of candidate options. Each conductor size is associated with distinct installation cost, maintenance cost, as well as specific power and current limits. The constraints are given by (14)-(16).

$$f_{ij}^{+}+f_{ij}^{-}=f_{ij}\quad\forall(i,j)\in B \tag{14}$$

$$f_{ij}=\sum_{a\in A}Y_{ij}^{a}\quad\forall(i,j)\in B \tag{15}$$

$$\begin{cases} s_{ij}^{a}=\sum_{a\in A}c_{a}^{\mathrm{conductor}}Y_{ij}^{a}\quad\forall(i,j)\in B \\ m_{ij}^{a}=\sum_{a\in A}c_{a}^{\mathrm{maintenance}}Y_{ij}^{a}\quad\forall(i,j)\in B \\ S_{ij}^{\max}=\sum_{a\in A}S_{a}^{\max}Y_{ij}^{a}\quad\forall(i,j)\in B \\ I_{ij}^{\max}=\sum_{a\in A}I_{a}^{\max}Y_{ij}^{a}\quad\forall(i,j)\in B \\ r_{ij}=\sum_{a\in A}r_{ij}^{a}Y_{ij}^{a}\quad\forall(i,j)\in B \\ x_{ij}=\sum_{a\in A}x_{ij}^{a}Y_{ij}^{a}\quad\forall(i,j)\in B \end{cases} \tag{16}$$

Constraint (14) shows whether the edge (i,j) transfers the fictitious power flow. $f_{ij}=1$ indicates that edge (i,j) is selected. Otherwise, $f_{ij}=0$ indicates that edge (i,j) is not selected. Equation (15) dictates that only one type of conductor size should be selected in the edge (i,j). Moreover, (16) implies that different conductor sizes have their corresponding unit costs and thermal stability limits. The binary variable Y_{ij}^{a} indicates that the edge (i,j) is equipped with the conductor type a.

C. Power Flow Constraints in Geographic Graph

In the geographic graph, the branch-based power flow constraints could be modified to edge-based power flow constraints, which are combined with the directional binary variables of fictitious power flow to meet the node power balance in (17)-(20) [16]. Apart from the convex constraints, each edge should also abide by the voltage constraints and thermal limits:

$$P_i^{\text{out}} = \sum_{(i,j)\in B_i^{\text{start}}} (P_{ij}^{+} - P_{ij}^{-} + I_{ij}^{-} r_{ij}) + \sum_{(i,j)\in B_i^{\text{end}}} (P_{ij}^{-} - P_{ij}^{+} + I_{ij}^{+} r_{ij}) \quad \forall i \in N \tag{17}$$

$$Q_i^{\text{out}} = \sum_{(i,j)\in B_i^{\text{start}}} (Q_{ij}^{+} - Q_{ij}^{-} + I_{ij}^{-} x_{ij}) + \sum_{(i,j)\in B_i^{\text{end}}} (Q_{ij}^{-} - Q_{ij}^{+} + I_{ij}^{+} x_{ij}) \quad \forall i \in N \tag{18}$$

$$P_i^{\text{g}} = P_i^{\text{out}} + P_i^{\text{load}} \quad \forall i \in N \tag{19}$$

$$Q_i^{\text{g}} = Q_i^{\text{out}} + Q_i^{\text{load}} \quad \forall i \in N \tag{20}$$

Equations (17) and (18) represent the active and reactive power outflows of each node through the edges connected to the node, respectively. Equations (19) and (20) concern the active and reactive source power inflows $(P_i^{\text{g}}, Q_i^{\text{g}})$ of each node, which should be equal to the sum of active and reactive power outflows $(P_i^{\text{load}}, P_i^{\text{out}}, Q_i^{\text{load}}, Q_i^{\text{out}})$ of the node, respectively.

$$-Mf_{ij}^{+} \le V_i - V_j + 2(P_{ij}^{+} r_{ij} + Q_{ij}^{+} x_{ij}) + I_{ij}^{+}(r_{ij}^2 + x_{ij}^2) \le Mf_{ij}^{+} \quad \forall (i,j) \in B \tag{21}$$

$$-Mf_{ij}^{-} \le V_j - V_i + 2(P_{ij}^{-} r_{ij} + Q_{ij}^{-} x_{ij}) + I_{ij}^{-}(r_{ij}^2 + x_{ij}^2) \le Mf_{ij}^{-} \quad \forall (i,j) \in B \tag{22}$$

$$\sqrt{4(P_{ij}^{+})^2 + 4(Q_{ij}^{+})^2 + (I_{ij}^{+} - V_i)^2} \le I_{ij}^{+} - V_j \quad \forall (i,j) \in B \tag{23}$$

$$\sqrt{4(P_{ij}^{-})^2 + 4(Q_{ij}^{-})^2 + (I_{ij}^{-} - V_j)^2} \le I_{ij}^{-} - V_i \quad \forall (i,j) \in B \tag{24}$$

Formulas (21)-(24) indicate the convex fictitious power flow constraints on each edge according to the second-order cone relaxation technique.

$$\begin{cases} -\sqrt{2}\, S_{ij}^{\max} \le (P_{ij}^{+} + P_{ij}^{-}) + (Q_{ij}^{+} + Q_{ij}^{-}) \le \sqrt{2}\, S_{ij}^{\max} & \forall (i,j) \in B \\ -\sqrt{2}\, S_{ij}^{\max} \le (P_{ij}^{+} + P_{ij}^{-}) - (Q_{ij}^{+} + Q_{ij}^{-}) \le \sqrt{2}\, S_{ij}^{\max} & \forall (i,j) \in B \\ P_{ij}^{+}, P_{ij}^{-} \in [0, S_{ij}^{\max}] & \forall (i,j) \in B \\ Q_{ij}^{+}, Q_{ij}^{-} \in [0, S_{ij}^{\max}] & \forall (i,j) \in B \end{cases} \tag{25}$$

$$\begin{cases} 0 \le I_{ij}^{+} + I_{ij}^{-} \le I_{ij}^{\max} & \forall (i,j) \in B \\ 0 \le I_{ij}^{+} \le Mf_{ij}^{+} & \forall (i,j) \in B \\ 0 \le I_{ij}^{-} \le Mf_{ij}^{-} & \forall (i,j) \in B \end{cases} \tag{26}$$

$$V_i^{\min} \le V_i \le V_i^{\max} \quad \forall i \in N \tag{27}$$

The appropriate conductor size would be determined by thermal stability constraints. As indicated in (25) and (26), the model adheres to these thermal stability limits, ensuring that both the power flow and current for each edge remain below their respective upper limits. Moreover, (27) establishes voltage constraints for each node.

IV. Model Improvement Using Affiliation Variables and Algebraic Formulas

A. Affiliation Variables

As proposed in [19] and [20], there may be a large number of downstream branches of a feeder in the distribution network. Similarly, there is also an upstream-downstream relationship of edges in the fictitious power flow, where the upstream-downstream relationship is represented by affiliation variables of edges k_{xy}^{ij} in the fictitious power flow model. For instance, $k_{xy}^{ij} = 1$ is used to represent that edge (x,y) is the downstream edge of edge (i,j). As shown in Fig. 3, a radial fictitious power flow is illustrated to clarify the use of affiliation variables. In Fig. 3, six edges are selected, and the affiliation variables of these six edges are shown in (28). In (29), $k_{ij}^{ij} = 1$ is applied when the edge (i,j) is selected in the fictitious power flow.

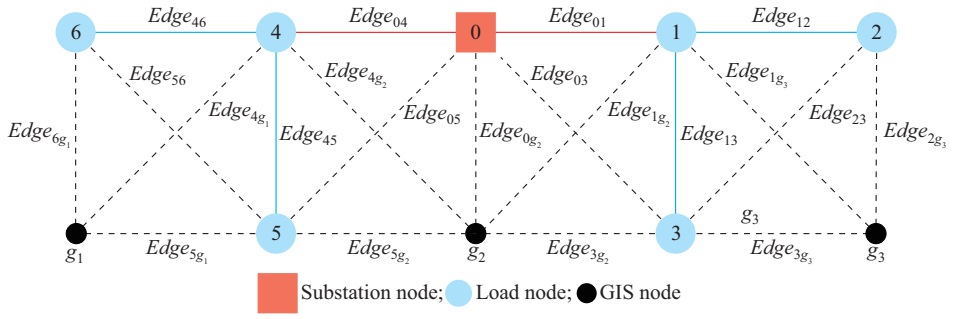

Fig. 3. Subordination between feeder and branches.

$$\begin{cases} k_{04}^{04} = k_{46}^{04} = k_{45}^{04} = 1 & Edge_{04} \\ k_{01}^{01} = k_{12}^{01} = k_{13}^{01} = 1 & Edge_{01} \\ k_{46}^{46} = k_{12}^{12} = k_{13}^{13} = k_{45}^{45} = 1 & Edge_{46,\,12,\,13,\,45} \end{cases} \tag{28}$$

To determine the affiliation variables in the optimization process, direction variables f_{ij}^{+}, f_{ij}^{-} of the fictitious power flow are added to the constraints. The affiliation variables-related constraints are expressed as:

$$k_{xy}^{ij} = 0 \quad \forall (i,j) \in B^{\text{source}}, \forall (x,y) \in B^{\text{source}}, (i,j) \ne (x,y) \tag{29}$$

$$\sum_{(i,j)\in B^{\text{source}}} \sum_{(x,y)\in B} k_{xy}^{ij} = \sum_{(i,j)\in B} f_{ij} \tag{30}$$

Referring to edges $Edge_{04}$ and $Edge_{01}$, (29) indicates that there is no affiliation of different edges connected to the source node. From (30), the sum of the downstream edges

of the edges connected to the source node is equal to the total number of edges applied in FR.

$$-Mf_{ij}^{+} \le \sum_{(x,y)\in B} k_{xy}^{ij} - \sum_{\substack{(j,z)\in B_j,\ (x,y)\in B \\ (i,j)\neq(j,z)}} k_{xy}^{jz} - 1 \le Mf_{ij}^{+} \quad \forall (i,j)\in B \tag{31}$$

$$-Mf_{ij}^{-} \le \sum_{(x,y)\in B} k_{xy}^{ij} - \sum_{\substack{(i,z)\in B_j,\ (x,y)\in B \\ (i,j)\neq(i,z)}} k_{xy}^{iz} - 1 \le Mf_{ij}^{-} \quad \forall (i,j)\in B \tag{32}$$

$$k_{ij}^{ij} = f_{ij} \quad \forall (i,j)\in B, i,j \notin N^{\text{source}} \tag{33}$$

$$k_{ij}^{xy} + k_{xy}^{ij} \le (f_{ij} + f_{xy})/2 \quad \forall (i,j)\in B, \forall (x,y)\in B, (i,j)\neq(x,y) \tag{34}$$

Formulas (31) and (32) indicate that the affiliation variable of edge (i,j) is one more than the total number of all affiliation variables of downstream edges connected to (i,j). In (33), once an edge (i,j) is selected in fictitious power flow, $k_{ij}^{ij} = 1$. Formula (34) ensures that the interrelationship of upstream and downstream between any two edges is disallowed.

B. Calculation of Reliability Indices

According to the algebraic reliability formula in [10], the reliability indices are constrained as:

$$\Gamma_i^{\text{RS}}, \Gamma_i^{\text{SO}}, \Pi_i^{\text{RS}}, \Pi_i^{\text{SO}} \in [0, Mn_i] \quad \forall i \in N \tag{35}$$

$$\Gamma_i^{\text{RS}} = \Pi_i^{\text{RS}} = \Gamma_i^{\text{SO}} = \Pi_i^{\text{SO}} = 0 \quad \forall i \in N^{\text{source}} \tag{36}$$

From (35), the reliability indices of the nodes not used in FR are constrained to be zero. For the nodes used in FR, the reliability indices are constrained to be greater than zero. However, the expected duration and rate of interruptions affecting source node i are constrained to be zero in (36) [21].

To estimate the reliability indices in the optimization process, the constraints on each edge are given as:

$$-Mf_{ij} \le \Gamma_j^{\text{RS}} - \Gamma_i^{\text{RS}} - \tau_{ij}^{\text{RS}} \lambda_{ij} d_{ij} (f_{ij}^{+} - f_{ij}^{-}) \le Mf_{ij} \quad \forall (i,j)\in B \tag{37}$$

$$-Mf_{ij} \le \Pi_j^{\text{RS}} - \Pi_i^{\text{RS}} - \lambda_{ij} d_{ij} (f_{ij}^{+} - f_{ij}^{-}) \le Mf_{ij} \quad \forall (i,j)\in B \tag{38}$$

$$-Mf_{ij} \le \Gamma_i^{\text{SO}} - \Gamma_j^{\text{SO}} - \tau_{ij}^{\text{RS}} \lambda_{ij} d_{ij} (f_{ij}^{+} - f_{ij}^{-}) \le Mf_{ij} \quad \forall (i,j)\in B\backslash B^{\text{source}} \tag{39}$$

$$-Mf_{ij} \le \Pi_i^{\text{SO}} - \Pi_j^{\text{SO}} - \lambda_{ij} d_{ij} (f_{ij}^{+} - f_{ij}^{-}) \le Mf_{ij} \quad \forall (i,j)\in B\backslash B^{\text{source}} \tag{40}$$

Formulas (37)-(40) indicate that the load-nodal reliability indices are constrained by the fictitious power flow direction variables, meaning that the reliability formulas on the edge (i,j) are available when the fictitious power flow direction variable is available ($f_{ij}^{+} = 1$ or $f_{ij}^{-} = 1$). However, since the expected nodal rate and durations of switching-only interruptions of the source nodes are equal to zero, the edges connected to the source nodes are not required to meet constraints (39) and (40).

As proposed in [10], Γ_i^{SO} and Π_i^{SO} of source nodes and their adjacent nodes are merely related to their downstream edges. These reliability indices are unable to be constrained by (39) and (40) due to $\Gamma_{\text{source}}^{\text{SO}} = 0$ and $\Pi_{\text{source}}^{\text{SO}} = 0$, respectively. Therefore, the proposed method improves the corresponding constraints based on the introduced affiliation variables. The improved constraints of edges connected to the source nodes are set as:

$$-Mf_{ij} \le \sum_{(x,y)\in B} \tau_{ij}^{\text{RS}} \lambda_{ij} d_{ij} k_{xy}^{ij} - \Gamma_j^{\text{SO}} - \tau_{ij}^{\text{RS}} \lambda_{ij} d_{ij} (f_{ij}^{+} - f_{ij}^{-}) \le Mf_{ij} \quad \forall (i,j)\in B^{\text{source}}, \forall i \in N^{\text{source}} \tag{41}$$

$$-Mf_{ij} \le \sum_{(x,y)\in B} \lambda_{ij} d_{ij} k_{xy}^{ij} - \Pi_j^{\text{SO}} - \lambda_{ij} d_{ij} (f_{ij}^{+} - f_{ij}^{-}) \le Mf_{ij} \quad \forall (i,j)\in B^{\text{source}}, \forall i \in N^{\text{source}} \tag{42}$$

To ensure the customized reliability requirements of the FR, different reliability constraints for load nodes are represented by:

$$CIF_i \le \varepsilon_i^{\text{CIF}} \quad \forall i \in N^{\text{load}} \tag{43}$$

$$CID_i \le \varepsilon_i^{\text{CID}} \quad \forall i \in N^{\text{load}} \tag{44}$$

C. Model Improvement

To determine which edges and vertices of the graph are applied in the FR, the fictitious power flow variables of edges and vertices are set to represent the states of edges and vertices. Specifically, these variables equal to 1 represent that the edges and vertices are used. Once they are equal to 0, it means that the edges and nodes are not used in the FR.

$$\sum_{i\in N} n_i - 1 = \sum_{(i,j)\in B} f_{ij} \tag{45}$$

$$n_i \ge f_{ij} \quad \forall (i,j)\in B_i, \forall i \in N \tag{46}$$

$$\begin{cases} V_i^{\min} = n_i V^{\min} \\ V_i^{\max} = n_i V^{\max} \end{cases} \quad \forall i \in N \tag{47}$$

$$P_i^{\text{out}}, Q_i^{\text{out}} \in [-Mn_i, Mn_i] \quad \forall i \in N \tag{48}$$

Equation (45) indicates that in the fictitious power flow model, the total number of discrete edges used is one less than the total number of discrete vertices, thereby satisfying the radial topology constraint. Formula (46) implies that the vertex i is used in the network when the fictitious power flow of the edges connected to vertex i is used. Equation (47) indicates that the upper and lower voltage limits are equal to the critical number when the vertices are used. Once the vertices are not used, the voltage upper and lower limits are equal to zero. Formula (48) indicates that the active and reactive power flowing out of the selected nodes is not limited, and the active and reactive power flowing out of the unapplied vertices is equal to zero.

For conductor sizing, the impedance should be set as variable, which is different for diverse conductor sizes in the optimization process. However, the resistance and reactance of each edge are unavailable to be set as variable (r_{ij}, x_{ij}) due to the inappropriate products of the variables such as $P_{ij}^{+} r_{ij}$, $Q_{ij}^{+} x_{ij}$, $I_{ij}^{+}(r_{ij}^2 + x_{ij}^2)$. Meanwhile, as demonstrated in [22], the MISOCP model demonstrates that the relaxation error remains consistently below 0.1% in FR optimization. This empirical evidence substantiates the mathematical tightness of the proposed model. Therefore, auxiliary variables such as Pr_{ij}^{+}, Qx_{ij}^{+}, Ir_{ij}^{+}, Ix_{ij}^{+} are introduced in the constraints as:

$$\begin{aligned} &Pr_{ij}^{+} - P_{ij}^{+} r_{ij}, Pr_{ij}^{-} - P_{ij}^{-} r_{ij}, Qx_{ij}^{+} - Q_{ij}^{+} x_{ij}, Qx_{ij}^{-} - Q_{ij}^{-} x_{ij}, Ir_{ij}^{+} - I_{ij}^{+} r_{ij}, \\ &Ir_{ij}^{-} - I_{ij}^{-} r_{ij}, Ix_{ij}^{+} - I_{ij}^{+} x_{ij}, Ix_{ij}^{-} - I_{ij}^{-} x_{ij}, Irx_{ij}^{+} - I_{ij}^{+}(r_{ij}^2 + x_{ij}^2), \\ &Irx_{ij}^{-} - I_{ij}^{-}(r_{ij}^2 + x_{ij}^2) \in [-M(1 - f_{ij}), M(1 - f_{ij})] \quad \forall (i,j)\in B \end{aligned} \tag{49}$$

$$\begin{cases} Pr_{ij}^{+}, Qx_{ij}^{+}, Ir_{ij}^{+}, Ix_{ij}^{+}, Irx_{ij}^{+} \in [0, Mf_{ij}^{+}] & \forall (i,j) \in B \\ Pr_{ij}^{-}, Qx_{ij}^{-}, Ir_{ij}^{-}, Ix_{ij}^{-}, Irx_{ij}^{-} \in [0, Mf_{ij}^{-}] & \forall (i,j) \in B \end{cases} \quad (50)$$

From (49) and (50), all the inappropriate products of variables are transformed into the products of variables and data sets (e.g., r_{ij}^{a}, x_{ij}^{a}). Based on the introduced auxiliary variables, (17), (18), (21), and (22) are improved, as represented in (51)-(54), respectively.

$$P_i^{\text{out}} = \sum_{(i,j) \in B_i^{\text{start}}} (P_{ij}^{+} - P_{ij}^{-} + Ir_{ij}^{-}) + \sum_{(i,j) \in B_i^{\text{end}}} (P_{ij}^{-} - P_{ij}^{+} + Ir_{ij}^{+}) \quad \forall i \in N \quad (51)$$

$$Q_i^{\text{out}} = \sum_{(i,j) \in B_i^{\text{start}}} (Q_{ij}^{+} - Q_{ij}^{-} + Ix_{ij}^{-}) + \sum_{(i,j) \in B_i^{\text{end}}} (Q_{ij}^{-} - Q_{ij}^{+} + Ix_{ij}^{+}) \quad \forall i \in N \quad (52)$$

$$-Mf_{ij}^{+} \le V_i - V_j + 2(Pr_{ij}^{+} + Qx_{ij}^{+}) + Irx_{ij}^{+} \le Mf_{ij}^{+} \quad \forall (i,j) \in B \quad (53)$$

$$-Mf_{ij}^{-} \le V_j - V_i + 2(Pr_{ij}^{-} + Qx_{ij}^{-}) + Irx_{ij}^{-} \le Mf_{ij}^{-} \quad \forall (i,j) \in B \quad (54)$$

V. Case Study

Two case studies based on a 28-node test system and a 160-node large system are conducted to verify the effectiveness and applicability of the fictitious power flow model. It is assumed that the permissible range of voltage is between 0.95 p.u. and 1.05 p.u.. Four types of candidate conductors are selected from [23] and [24] including Gopher, Ferret, Mink, and Raccoon. The cost coefficient for EENS μ is set to be 11200 $/MWh, and the mean value of the reliability cost of all the fictitious power flows from different source nodes is set as part of the objective function. Moreover, we assume that the annual load growth rate of each load node is 5% and the feeder operation period is 20 years. The optimization model is solved by the Gurobi solver on a 2.9 GHz personal computer with 16 GB of RAM.

A. 28-node Test System

The 28-node test system contains 28 vertices and 81 edges, which is used to illustrate the impact of including reliability and geographic constraints in the FR optimization. Figure 4 shows the FR results. Nine load nodes are represented by blue circles and two power source nodes are represented by red squares. The geographical distribution of power source nodes and load nodes is shown in Fig. 4(a). The horizontal lengths of the edges are 1 km or $\sqrt{2}$ km for non-crossing edges or crossing edges, respectively. Vertical height is assumed to be the same in this case study. The interruption rate of each edge is set to be 0.1 per year per kilometer [21]. And the interruption durations for repair-and-switching and switching-only cases are set to be 3 hours and 0.5 hours, respectively [6]. There are three load levels in reliability estimation. Loading factors of load levels 1, 2, and 3 are 70%, 83%, and 100%, respectively, and durations of load levels 1, 2, and 3 are 2000 hours, 5760 hours, and 1000 hours, respectively.

To verify the availability, the FR, conductor sizing, and simultaneous reliability evaluation are made in the test case. The fictitious power flows of different source nodes and spatial network layout are determined in the optimization process. In more details, the fictitious power flows 1 and 2 of two source nodes are shown in Fig. 4(b) and Fig. 4(c), respectively. Based on the superimposed fictitious power flow, the distribution network is constructed for the two power source nodes in Fig. 4(d). The results show that the operating fictitious power flow is radial, but the network is of mesh type.

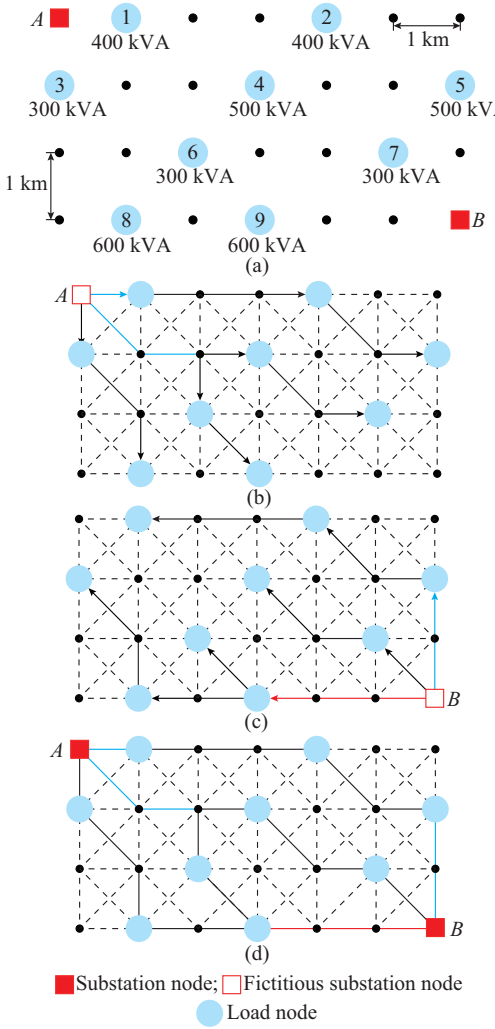

Fig. 4. FR results for 28-node test system. (a) Geographical distribution of source nodes and load nodes. (b) Fictitious power flow of source A. (c) Fictitious power flow of source B. (d) Mesh distribution network structure.

The reliability indices are summarized in Table II, while the fictitious power flow results are presented in Table III. Additionally, Tables IV provides the conductor sizes and associated costs of the feeder. The reliability indices (CIF and CID) under $N-1$ failure in different fictitious power flows are shown in Table II, which are evaluated under the repair-and-switching interruptions and switching-only interruptions. In Table II, the CID of node 3 is 0.421 hour/year in the fictitious power flow 1. But the CID at node 3 of fictitious power flow 2 is 2.254 hour/year and maximal among all the nodes. In this test case, CIF is constrained to be less than 0.8 interruption/year and CID is constrained to be less than 2.5 hour/year. As shown in Table II, the CIF and CID indicators of all nodes meet the set constraints. Moreover, SAIFI, SAIDI, ASAI, and EENS of fictitious power flow from source nodes 1 and 2 are 0.60 interruption/year, 1.26 hour/

year, 99.999%, 4.015 MWh/year, and 0.69 interruption/year, 1.40 hour/year, 99.984%, and 4.4754 MWh/year, respectively. It can be observed that reliability indices of the planned network can be precisely calculated in the FR.

TABLE II
RELIABILITY INDICES OF $N-1$ FAILURE

Load node	Fictitious power flow 1		Fictitious power flow 2	
	CIF (interruption/year)	CID (hour/year)	CIF (interruption/year)	CID (hour/year)
1	0.641	0.571	0.741	2.224
2	0.641	1.321	0.741	1.474
3	0.341	0.421	0.800	2.254
4	0.700	1.266	0.383	1.149
5	0.641	1.924	0.741	0.871
6	0.700	1.204	0.800	1.504
7	0.700	1.807	0.383	0.545
8	0.341	1.024	0.800	1.650
9	0.700	1.557	0.800	1.150

TABLE III
COMPARISON OF FICTITIOUS POWER FLOWS OF DIFFERENT SOURCE NODES

Source node	Edge	Co-contained edge
Source node 1	$\{l_1, l_2, l_3, l_{29}, l_{33}, l_{35}\}$, $\{l_4, l_8, l_{12}, l_{19}, l_{28}, l_{40}, l_{45}, l_{56}, l_{61}, l_{66}\}$	$l_4, l_8, l_{12}, l_{19}, l_{28}, l_{40}, l_{45}, l_{56}, l_{61}, l_{66}$
Source node 2	$\{l_{50}, l_{73}, l_{75}, l_{77}, l_{78}, l_{79}, l_{80}, l_{81}\}$, $\{l_4, l_8, l_{12}, l_{19}, l_{28}, l_{40}, l_{45}, l_{56}, l_{61}, l_{66}\}$	$l_4, l_8, l_{12}, l_{19}, l_{28}, l_{40}, l_{45}, l_{56}, l_{61}, l_{66}$

TABLE IV
CONDUCTOR TYPES OF FR

Conductor type	Edge of FR	Number of edges	Installation cost of conductor (k$)
Gopher	$l_2, l_4, l_8, l_{12}, l_{19}, l_{28}, l_{33}, l_{35}, l_{40}, l_{45}, l_{56}, l_{61}, l_{66}, l_{73}, l_{77}, l_{78}$	16	37.949
Ferret	$l_1, l_3, l_{29}, l_{50}, l_{75}$	5	18.408
Mink	l_{79}, l_{80}, l_{81}	3	15.000
Raccoon		0	0

From Table III, there are multiple repeatedly selected edges such as l_4, l_8, l_{12}, l_{19}, l_{28}, l_{40}, l_{45}, l_{56}, l_{61}, l_{66} of the two fictitious power flows. These edges are applied to transmit power in opposite directions of the two fictitious power flows, respectively. Moreover, based on the repeatedly selected edges, the FR of two substations will be connected together to meet the mesh requirement on the graph.

From Table IV, three types of conductor sizes are chosen based on conductor sizing analysis, where the installation cost of the Gopher type is the highest among all the conductor sizes. Generally, the conductor capacity of edges is determined by the maximum fictitious power flow through itself. The higher the conductor capacity is, the higher the cost of the conductor will be. However, to improve the economic performance, the conductor size with a lower unit cost such as Gopher is most adopted, even its thermal stability limit and capacity are not relatively high.

Considering the customized reliability requirements of different load demands, diverse reliability conditions can be applied to load nodes by constraining the reliability variables. Four reliability standards, namely A, B, C, and D, are specified as follows. Standards A, B, C, and D indicate that CID cannot exceed 2.7, 2.6, 2.5, and 2.4 hour/year, respectively; and CIF cannot exceed 1.2, 1.1, 1.0, and 0.9 interruption/year, respectively. In Table V, the associated costs such as installation cost, maintenance cost, and reliability cost of standard A are \$66943, \$38042, and \$20210, respectively, whose total cost is the least. Moreover, as the reliability constraints become stricter, the cost of FR increases. Consequently, the additional investment of FR can improve the reliability, and customized reliability requirements can be satisfied by the proposed method.

TABLE V
COSTS OF FR OF DIFFERENT RELIABILITY STANDARDS

Standard	Installation cost c_{I} (k$)	Maintenance cost c_{M} (k$)	Reliability cost c_{R} (k$)	Total cost (k$)
A	66.943	38.042	20.21	125.195
B	67.466	38.755	19.21	125.431
C	68.320	40.582	17.64	126.542
D	70.337	41.487	16.86	128.684

B. 160-node Large System

To illustrate the impact of reliability requirement and the presence of geographical obstacles in the FR, the fictitious power flow model is applied on a realistic 160-node large system [5]. Moreover, the performance of the proposed method has also been compared with the resilient FR method based on the radial layout presented in [5], where the mesh principle is ignored. In the geographic graph, the edges on the obstacle terrain are unable to be applied in the FR problem, resulting in the decrease of the number of available edges. As the number of available edges and the scale of the problem decrease, the speed and efficiency of obtaining the solution increase. In Fig. 5(a), a geographic graph is composed of 160 vertices and 564 edges, where the special terrains (such as green land and lakes) are marked as irregular-colored blocks. Affected by the terrain conditions, there are 132 edges restricted by the obstacles.

For the sake of simplicity and without loss of generality, the customized reliability requirement and the presence of geographical obstacles are analyzed in three cases.

1) Case 1: ignoring the impact of obstacle terrain, the fictitious power flow model would be solved on the graph with 160 nodes and 564 edges, where the optimal objective function value obtained without reliability consideration only contains the installation cost c_I and the maintenance cost c_M.

2) Case 2: considering the impact of obstacle terrain, 132 edges should be restricted by the obstacles. The available 432 edges will be selected and equipped with diverse conductor sizes for improving the total cost excluding the reliability cost c_R and solution efficiency.

3) Case 3: the impact of obstacle terrain is the same as that in Case 2, and only 432 edges are available on the graph. Besides, to reflect the effect of reliability consideration, the ASAI is constrained to be above 99.9% and the reliability cost c_R is also added to the total cost in this case.

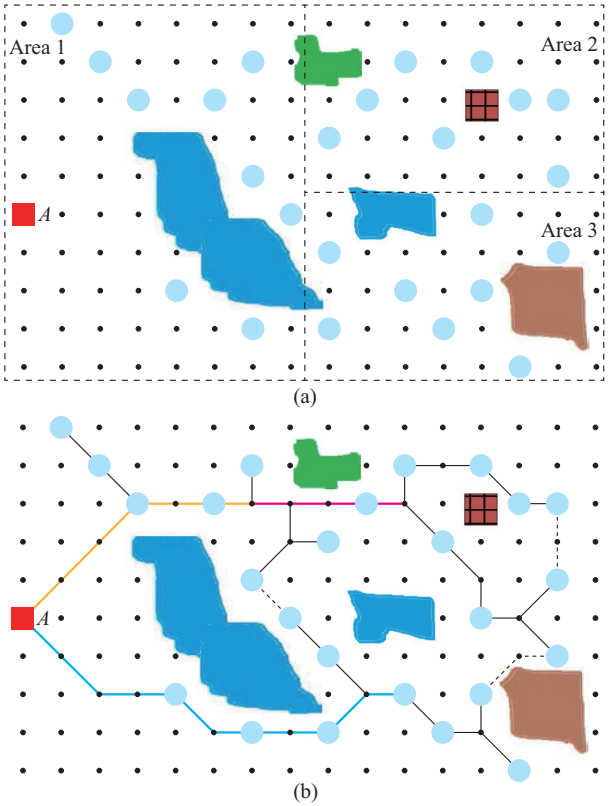

Fig. 5. FR result for 160-node large system. (a) Geographic graph of FR planning. (b) Optimal FR and conductor sizing.

The total costs in Cases 1 and 2 of the model based on [5] are obtained by replacing the conductor data with four types of candidate conductors provided in [5]. However, the total cost in Case 3 is unable to be obtained since the model based on [5] ignores the reliability cost. Moreover, the simulation time of the fictitious power flow model closely matches that of the model based on [5]. The comparison of total costs and simulation time are shown in Table VI.

TABLE VI
COMPARISON OF TOTAL COSTS AND SIMULATION TIME

Case	Model based on [5]		Fictitious power flow model	
	Total cost (M$)	Simulation time (min)	Total cost (M$)	Simulation time (min)
Case 1	1.057	32.0	0.93	40.0
Case 2	1.139	10.1	1.01	15.1
Case 3			1.03 + 0.25 = 1.28	12.0

From Table VI, the total costs in Case 1 and Case 2 obtained from the proposed model are 0.93 M$ and 1.01 M$, respectively, where the total cost in the presence of obstacles is higher because the geographical alternatives are more restricted. Moreover, the simulation time in Case 2 is much shorter due to the fewer binary variables and constraints compared with that in Case 1. Under the same condition of geographic obstacles in Case 2, the total cost yielded by the proposed model is lower but the simulation time is longer than that of the model based on [5]. In Case 3, the optimal FR and conductor sizing are shown in Fig. 5(b), where different conductor sizes are represented by solid lines of different colors (yellow for gopher-type conductors, pink for ferret-type, blue for mink-type, and black for raccoon-type). To meet the customized reliability requirement, several tie-lines marked with black dashed edges are applied in the FR. The total cost with consideration of reliability requirement is 1.28 M$, comprising 1.03 M$ of conductor investment cost and 0.25 M$ of reliability costs.

The 160-node large system is divided into three distinct areas, as illustrated in Fig. 5(a). Each area is characterized by unique compositions of distributed resources and load. Within each area, the load nodes exhibit the same load profiles, which are detailed in Fig. 6. The optimal FR results are comparatively analyzed in Fig. 5(b) and Fig. 7. Figure 5(b) presents the FR and conductor sizing solutions derived without load coincidence considerations, whereas Fig. 7 represents the result considering the load coincidence factor. This comparison demonstrates that the probabilistic load behavior indeed causes modifications in conductor sizing in the FR optimization.

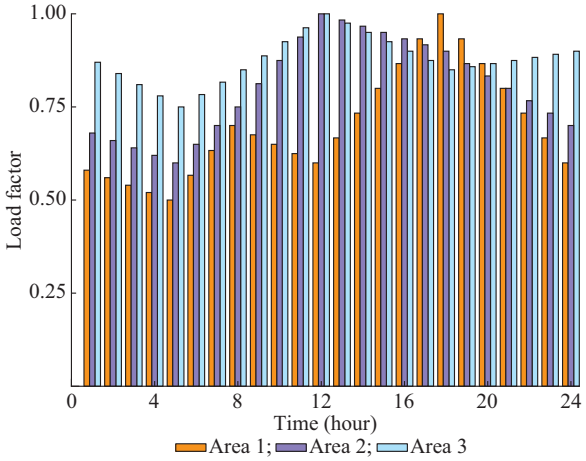

Fig. 6. Load profiles for 160-node large system.

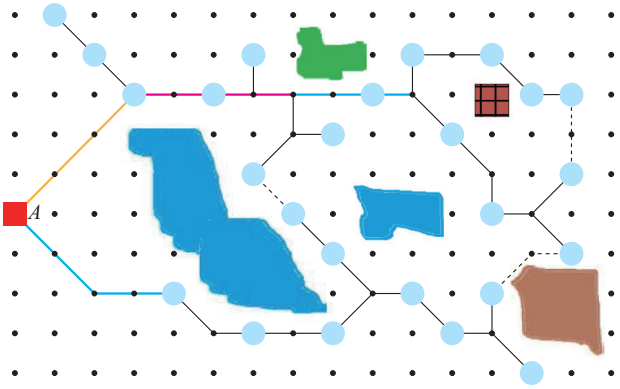

Fig. 7. Result considering load coincidence factor.

VI. CONCLUSION

In this paper, a reliability-centered planning method with geographic graph constraints is presented, which determines the spatial network layout and selects the conductor size to meet differentiated reliability requirements and improve the economic performance. In the proposed method, geographic graph constraints improve the FR to ensure the validity of planned FR. The overlapping feeder routes powered by ficti-

tious power flows from multiple sources are used to determine the line connection, which supersedes the general radial constraint with practical mesh network layout. The verification of fictitious power flow ensures the operational security of distribution networks. Besides, the calculation of reliability indices is achieved by introducing affiliation variables and algebraic formulas, effectively improving the spatial network layout. Compared with existing methods, the proposed method achieves cost-effective FR and conductor sizing, improving the economic performance of distribution network while adapting the FR constraints to the real geographical environment. In addition, the inclusion of reliability-related constraints in the planning process ensures the compliance with customized reliability requirements. The calculated reliability indices assist system designers in evaluating the performance of FR results, enabling decision-makers to make informed choices based on accurate models and analytical results.

REFERENCES

[1] A. Samui, S. Singh, T. Ghose *et al*., "A direct approach to optimal feeder routing for radial distribution system," *IEEE Transactions on Power Delivery*, vol. 27, no. 1, pp. 253-260, Jan. 2012.

[2] I. Ziari, G. Ledwich, A. Ghosh *et al*., "Optimal distribution network reinforcement considering load growth, line loss, and reliability," *IEEE Transactions on Power Systems*, vol. 28, no. 2, pp. 587-597, May 2013.

[3] N. G. Boulaxis and M. P. Papadopoulos, "Optimal feeder routing in distribution system planning using dynamic programming technique and GIS facilities," *IEEE Transactions on Power Delivery*, vol. 17, no. 1, pp. 242-247, Jan. 2002.

[4] C. M. Domingo, T. G. S. Roman, A. Sanchez-Miralles *et al*., "A reference network model for large-scale distribution planning with automatic street map generation," *IEEE Transactions on Power Systems*, vol. 26, no. 1, pp. 190-197, Feb. 2011.

[5] M. Mehrtash, A. Kargarian, and A. J. Conejo, "Graph-based second-order cone programming model for resilient feeder routing using GIS data," *IEEE Transactions on Power Delivery*, vol. 35, no. 4, pp. 1999-2010, Aug. 2020.

[6] R. C. Lotero and J. Contreras, "Distribution system planning with reliability," *IEEE Transactions on Power Delivery*, vol. 26, no. 4, pp. 2552-2562, Oct. 2011.

[7] F. J. Ruiz-Rodriguez, M. Gómez-González, and F. Jurado, "A method for reliability optimization of distributed generation using meta-heuristic and probabilistic techniques," *Electric Power Components and Systems*, vol. 43, no. 1, pp. 32-43, Nov. 2014.

[8] G. Munoz-Delgado, J. Contreras, and J. M. Arroyo, "Distribution network expansion planning with an explicit formulation for reliability assessment," *IEEE Transactions on Power Systems*, vol. 33, no. 3, pp. 2583-2596, May 2018.

[9] Z. Li, W. Wu, B. Zhang *et al*., "Analytical reliability assessment method for complex distribution networks considering post-fault network reconfiguration," *IEEE Transactions on Power Systems*, vol. 35, no. 2, pp. 1457-1467, Mar. 2020.

[10] A. Tabares, G. Munoz-Delgado, J. F. Franco *et al*., "An enhanced algebraic approach for the analytical reliability assessment of distribution systems," *IEEE Transactions on Power Systems*, vol. 34, no. 4, pp. 2870-2879, Jul. 2019.

[11] G. Munoz-Delgado, J. Contreras, and J. M. Arroyo, "Reliability assessment for distribution optimization models: a non-simulation-based linear programming approach," *IEEE Transactions on Smart Grid*, vol. 9, no. 4, pp. 3048-3059, Jul. 2018.

[12] M. Jooshaki, A. Abbaspour, M. Fotuhi-Firuzabad *et al*., "A MILP model for incorporating reliability indices in distribution system expansion planning," *IEEE Transactions on Power Systems*, vol. 34, no. 3, pp. 2453-2456, May 2019.

[13] J. R. Fletcher, T. Fernando, H. H.-C. Iu *et al*., "Spatial optimization for the planning of sparse power distribution networks," *IEEE Transactions on Power Systems*, vol. 33, no. 6, pp. 6686-6695, Nov. 2018.

[14] Z. Wang, D. Lin, G. Zeng *et al*., "A practical large-scale distribution network planning model based on elite Ant-Q," *IEEE Access*, vol. 8, pp. 58912-58922, Mar. 2020.

[15] M. Wang, M. Yang, Z. Fang *et al*., "A practical feeder planning model for urban distribution system," *IEEE Transactions on Power Systems*, vol. 38, no. 2, pp. 1297-1308, Mar. 2023.

[16] J. Shu, L. Wu, Z. Li *et al*., "A new method for spatial power network planning in complicated environments," *IEEE Transactions on Power Systems*, vol. 27, no. 1, pp. 381-389, Feb. 2012.

[17] Z. Lin, Z. Hu, and Y. Song, "Distribution network expansion planning considering $N-1$ criterion," *IEEE Transactions on Power Systems*, vol. 34, no. 3, pp. 2476-2478, May 2019.

[18] M. Jooshaki, A. Abbaspour, M. Fotuhi-Firuzabad *et al*., "MILP model of electricity distribution system expansion planning considering incentive reliability regulations," *IEEE Transactions on Power Systems*, vol. 34, no. 6, pp. 4300-4316, Nov. 2019.

[19] Z. Li, W. Wu, X. Tai *et al*., "A reliability-constrained expansion planning model for mesh distribution networks," *IEEE Transactions on Power Systems*, vol. 36, no. 2, pp. 948-960, Mar. 2021.

[20] C. Wang, K. Pang, M. Shahidehpour *et al*., "Flexible joint planning of sectionalizing switches and tie lines among distribution feeders," *IEEE Transactions on Power Systems*, vol. 37, no. 2, pp. 1577-1590, Mar. 2022.

[21] A. Bosisio, A. Berizzi, E. Amaldi *et al*., "Optimal feeder routing in urban distribution networks planning with layout constraints and losses," *Journal of Modern Power Systems and Clean Energy*, vol. 8, no. 5, pp. 1005-1014, Sept. 2020.

[22] H. Gao, J. Liu, L. Wang *et al*., "Cutting planes based relaxed optimal power flow in active distribution systems," *Electric Power Systems Research*, vol. 143, pp. 272-280, Feb. 2017.

[23] Z. Zhao and J. Mutale, "Optimal conductor size selection in distribution networks with high penetration of distributed generation using adaptive genetic algorithm," *Energies*, vol. 12, p. 2065, May 2019.

[24] O. D. Montoya, A. Garces, and C. A. Castro, "Optimal conductor size selection in radial distribution networks using a mixed-integer non-linear programming formulation," *IEEE Latin America Transactions*, vol. 16, no. 8, pp. 2213-2220, Aug. 2018.

Zhengbo Li received the M.S. degree in electrical engineering from Sichuan University, Chengdu, China, in 2023. He is currently pursuing the Ph.D. degree in electrical engineering at Sichuan University. His research interests include automatic planning for distribution network based on artificial intelligence, expansion planning of distribution network, and feeder routing.

Youbo Liu received the B.S., M.S., and Ph.D. degrees in electrical engineering from Sichuan University, Chengdu, China, in 2005, 2008, and 2011, respectively. He is currently a Professor with the College of Electrical Engineering, Sichuan University. His research interests include application of artificial intelligence in power system, optimization of AC/DC hybrid distribution network, and smart grid.

Yue Xiang received the Ph.D. degree in electrical engineering from Sichuan University, Chengdu, China, in 2016. He is currently a Professor with the College of Electrical Engineering, Sichuan University. His research interests include Energy Internet, smart grid, and integration of electric vehicle into power system.

Haolan Yang received the M.S. degree in power engineering and engineering thermophysics from Southeast University, Nanjing, China, in 2021. He is currently pursuing the Ph.D. degree in electrical engineering at Sichuan University, Chengdu, China. His research interests include artificial intelligence (AI)-powered and physics-informed methods for automatic operation of distribution network.

Lingfeng Wang received the Ph.D. degree in electrical & computer engineering from Texas A&M University, College Station, USA, in 2008. He is a Professor with the Department of Electrical Engineering and Computer Science, University of Wisconsin-Milwaukee, Milwaukee, USA. His research interests include power system and smart grid, and cyber security in energy system.

Junyong Liu received the Ph.D. degree in electrical engineering from Brunel University, London, UK, in 1998. He has been a Full Professor and Ph.D. supervisor with the College of Electrical Engineering and Information Technology, Sichuan University, Chengdu, China, since 1998. His research interests include smart energy, ecological agriculture, and electricity market.